Spherule layers, crater scaling laws, and the population of ancient terrestrial impactors

Brandon C. Johnson[1,2], Gareth S. Collins[3], David A. Minton[4], Timothy J. Bowling[4], Bruce M. Simonson[5], and Maria T. Zuber[1]

Affiliations:

[1] Department of Earth, Atmospheric and Planetary Sciences, Massachusetts Institute of Technology, 77 Massachusetts Avenue, Cambridge, MA 02139, USA.

[2] Now at: Department of Earth, Environmental and Planetary Sciences, Brown University, 324 Brook Street, Providence, RI 02912, USA.

[3]Impacts and Astromaterials Research Centre, Dept. Earth Science and Engineering, Imperial College London, London SW7 2AZ, UK

[4]Department of Earth, Atmospheric, and Planetary Sciences, Purdue University, 550 Stadium Mall Drive, West Lafayette, IN 47907, USA.

[5]Geology Department, Oberlin College, Oberlin, Ohio 44074, USA.

Revision for submission to *Icarus*, February 8th 2015

Keywords: Cratering; Earth; Moon; Near-Earth objects; Planetary dynamics

Abstract

Ancient layers of impact spherules provide a record of Earth's early bombardment history. Here, we compare different bombardment histories to the spherule layer record and show that 3.2-3.5 Ga the flux of large impactors (10-100 km in diameter) was likely 20-40 times higher than today. The E-belt model of early Solar System dynamics suggests that an increased impactor flux during the Archean is the result of the destabilization of an inward extension of the main asteroid belt (Bottke, W.F., Vokrouhlický, D., Minton, D., Nesvorný, D., Morbidelli, A., Brasser, R., Simonson, B., Levison, H.F., 2012. Nature 485, 78–81). Here, we find that the nominal flux predicted by the E-belt model is 7-19 times too low to explain the spherule layer record. Moreover, rather than making most lunar basins younger than 4.1 Gyr old, the nominal E-belt

29 model, coupled with a corrected crater diameter scaling law, only produces two lunar
30 basins larger than 300 km in diameter. We also show that the spherule layer record when
31 coupled with the lunar cratering record and careful consideration of crater scaling laws
32 can constrain the size distribution of ancient terrestrial impactors. The preferred
33 population is main-belt-like up to ~50 km in diameter transitioning to a steep distribution
34 going to larger sizes.
35
36 **1. Introduction**
37 The constant recycling of Earth's crust by plate tectonics makes it impossible to use
38 observations of terrestrial craters to determine if and how the impactor flux changed
39 throughout Earth's history (Johnson and Bowling, 2014). Fortunately, very large impacts
40 create distal ejecta layers with global extent (Smit, 1999). Even when the source crater
41 has been destroyed, these layers can act as a record of the impacts that created them
42 (Simonson and Glass, 2004). Although some impact ejecta layers are more proximal
43 material transported as part of the ballistic ejecta curtain, many of the layers are distal
44 deposits produced by impact (vapor) plumes (Glass and Simonson, 2012; Johnson and
45 Melosh, 2014; 2012a; Simonson and Glass, 2004). Estimates of the size of the impactors
46 that created these impact plume layers suggest that the impactor flux was significantly
47 higher 2.4-3.5 Ga than it is today, although these flux estimates are mostly qualitative
48 (Johnson and Melosh, 2012b).
49
50 The Early Archean to earliest Paleoproterozoic spherule layers formed well after the Late
51 Heavy Bombardment (LHB) (because almost all the layers are Early or Late Archean in

age, we refer to them collectively as Archean from here on for the sake of convenience). The LHB is thought to have ended after the formation of the lunar basin Orientale, about 3.7 Ga (Stöffler and Ryder, 2001). The Nice model is a dynamical model of the evolution of the orbits of the outer giant planets that has been used to explain the LHB through a destabilization of the main asteroid belt by abrupt migration of the giant planets (Gomes et al., 2005). The E-belt model, which includes an inward extension of the main asteroid belt from about 1.7-2.1 AU, was developed to explain the formation of the Archean spherule layers (Bottke et al., 2012).

Bottke et al. (2012) compare the expected number of Chixculub-sized craters on Earth over the timespans where spherule-bearing sedimentary sequences have been found in the Archean. The E-belt model assumes 6 km diameter bodies striking at 22 km/s create "Chicxulub sized" (~160-km diameter) craters on Earth (Bottke et al., 2015). According to Johnson and Melosh (2012b), a 6-km diameter impactor would make a sparse spherule layer only 0.09-0.2-mm thick. However, the observed Archean spherule layers are centimeters to 10's of centimeters thick and were likely created by impactors that are ~10-90 km in diameter (Johnson and Melosh, 2012b; Kyte et al., 2003; Lowe et al., 2003, 2014; Lowe and Byerly, 2015). In section 2, using the method of Johnson and Melosh (2012b), we estimate the sizes of the impactors that created each of the Archean spherule layers. We then compare this record to different possible bombardment histories. We find that the nominal flux predicted by the E-belt model is 7-19 times too low to produce the Archean spherule layers.

In section 3 we show that careful application of crater scaling laws provides a reasonably consistent relationship (<10% discrepancy) between crater size and impactor properties that is in excellent agreement with recent numerical models of terrestrial crater formation. Then, as an additional test of the E-belt model, we calculate the impactor size required to produce a 160-km diameter "Chicxulub sized" crater on Earth. Contrary to the 6 km diameter impactor estimate of Bottke et al. (2012), a ~13 km diameter impactor is required to produce a 160-km diameter crater on Earth at an impact speed of ~22 km/s. The approximately factor of two discrepancy in impactor size implies that the Bottke et al. (2012) E-belt flux is overestimated by a factor of 7.5-10. In this scenario, the nominal E-belt model produces only two craters larger than 300 km in diameter on the Moon rather than most of the LHB basins (Bottke et al., 2012; Morbidelli et al., 2012).

Finally in section 4 we combine constraints on the impactor Size Frequency Distribution (SFD) with constraints from the lunar cratering record. We find that the population of ancient impactors that is roughly main-belt like from ~1-30 km in diameter but steeper than the main-belt SFD at larger sizes is consistent with the lunar cratering record and the terrestrial impact record from spherule layers.

2. Spherule layer constraints on Terrestrial bombardment

Observations of NEOs provide a direct estimate of the present-day impactor flux (Figure 1; Stuart and Binzel, 2004). For objects greater than 10 km in diameter, these estimates suffer from small number statistics. Because asteroids larger than ~10 km in diameter are delivered to the NEO population predominantly by the size-independent effect of

dynamical chaos, we expect little difference between NEO and main-belt size distributions for objects larger than 10 km in diameter (Minton and Malhotra, 2010). Thus, we scale the main-belt SFD (Minton et al., 2015b) to be equal to the NEO SFD for a 10-km diameter object (Figure 1). We then assume the actual current impactor flux is the maximum of these two curves, which is a similar method to that used by Le Feuvre and Wieczorek (2011). This combined impactor SFD allows us to compare different bombardment histories to the spherule layer record, which predicts some impactors were substantially larger than 30 km in diameter. We note that the size above which we expect the impactor SFD to appear main-belt like is not strictly constrained. Additionally, there is only a small size range where both distributions are well determined (ie. the main belt population is poorly constrained for bodies smaller than a few km in diameter while above a few km in size the NEO population suffers from poor statistics). However, the errors associated with flux estimates based on the spherule layer record are likely much larger than any uncertainty associated with our estimates of the current day impactor SFD.

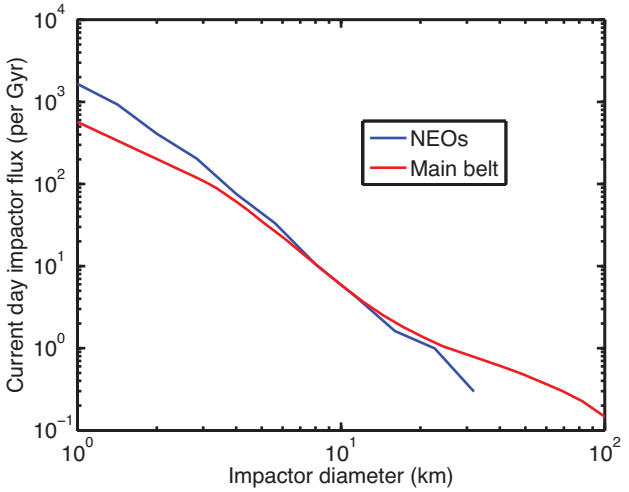

Figure 1: The cumulative rate of impacts larger than a given size as a function of impactor diameter. The blue curve is the current impactor flux based on observations of NEOs (Stuart and Binzel, 2004). We note that the impactor flux estimates of Stuart and Binzel (2004) are in excellent agreement with more recent estimates in this size range (Harris and D'Abramo, 2015). The red curve is the main belt asteroid belt size frequency distribution (Minton et al., 2015b) scaled so that it is equal to the impactor flux of NEOs for bodies with 10 km diameter.

Figure 2 shows the cumulative number of impacts by bodies larger than 10 km in diameter for three bombardment histories. The decreasing flux estimate is based on dynamical erosion of the asteroid belt (Minton and Malhotra, 2010) and is scaled so that the current impactor flux is equal to the impactor flux calculated based on observations of NEOs (Stuart and Binzel, 2004). One minor difference between this work and that of Minton and Malhotra (2010) is that we have shifted the starting time of the decay of the main asteroid belt from 4.0 Ga to 4.5 Ga. Because we normalize the flux rate so that the current flux is equal to the estimates based on NEO observations, this change only reduces the flux estimates by a factor of less than two during the times of interest. The impact velocity of 22 km/s for E-belt impactors (Bottke et al., 2015; 2012) is not significantly different from 20.3 km/s, the mean impact velocity of asteroids impacting the Earth (Minton and Malhotra, 2010). According to Equation 1, this difference in

138 impact velocity only changes the transient crater size by 3.6%. Thus, we can safely
139 ignore the slightly higher velocity of E-belt impactors and directly compare the number
140 of impacting bodies of a given size when comparing different flux estimates.
141
142 The nominal E-belt model assumes that destabilization of the E-belt occurs 4.1 Ga,
143 however, this timing is not strictly constrained (Bottke et al., 2012; Morbidelli et al.,
144 2012). In the context of the Nice model, a destabilization of the E-belt 3.9 Ga
145 corresponds to the lunar cataclysm view of the LHB, where almost all lunar basins
146 formed about 3.9 Ga (Morbidelli et al., 2012). Moving the destabilization any later than
147 that would imply that the Nice model cannot explain the LHB. Thus, we include flux
148 estimates for destabilization at 4.1 Ga and 3.9 Ga to encompass the entire range of
149 possible destabilization times (Figure 2).
150
151
152
153
154

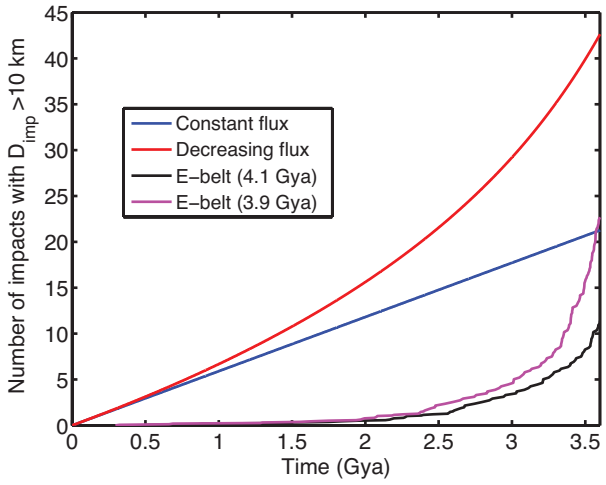

Figure 2: Cumulative number of impactors larger than 10 km in diameter that hit the Earth. The blue line is calculated assuming a constant impactor flux equal to the current impactor flux (Stuart and Binzel, 2004). The red curve assumes the constantly decreasing impactor flux estimated by Minton and Malhotra (2010). The flux rate from Minton and Malhotra (2010) is normalized so that the current flux is equal to the estimates based on NEO observations (Stuart and Binzel, 2004). The purple and black curves are the cumulative number of "E-belt" impactors assuming a destabilization at 3.9 Ga and 4.1 Ga, respectively (Bottke et al., 2012). Note that the E-Belt impact curves were generated using a very simple model for the migration of the giant planets, and therefore the decay curves could potentially be different if a more realistic evolution of the outer planets were considered. Note that including impacts out to 3.9 Gya, the cumulative bombardment from the nominal E-belt model (purple) exceeds the the value implied by a decreasing main belt flux (red) by a factor of 2.6.

As Table 1 shows, the age of the ancient spherule layers cluster between 2.49-2.63 Ga and 3.23-3.47 Ga. To compare the flux to the number of spherule layers, we assume that the clustering is purely the result of strata from these two periods being well searched and particularly suited to preserving spherule layers. The average time between large impacts is about 0.05 Gyr between 2.49-2.63 Ga and about 0.03 Gyr between 3.23-3.47 Ga. To account in some crude way for the fact that impacts are Poisson distributed we add the average recurrence rate to both sides of the respective period. More precisely we assume the spherule layer record is complete between 2.44-2.68 Ga and 3.2-3.5 Ga. This means that there may be several undiscovered, destroyed, or obscured layers that formed

between 2.68-3.2 Ga, but that we have found all of the layers that formed between 2.44-2.68 Ga and 3.2-3.5 Ga. We note this assumption may produce a conservative estimate of impactor flux because there may be more layers within the strata that have already been searched. For example, Mohr-Westheide et al. (2015) and Koeberl et al. (2015a,b) report on newly discovered Early Archean spherule layers in South Africa that may be distinct from any of those previously reported by Lowe et al. (2003, 2014).

Name	Approximate age (Ga)	Aggregate thickness (cm)	Impactor Diameter (km)
Dales Gorge & Kuruman	2.49	0.5-6	11-39
Bee Gorge	2.54	1-3	13-31
Reivilo & Paraburdoo	2.54-2.56	2-2.5	17-29
Jeerinah, Carawine, & Monteville	2.63	0.4-30	10-67
S5	3.23	20-50	37-79
S4	3.24	12	31-49
S3	3.24	30	42-67
S2	3.26	10-70	29-88
S6	3.26-3.30	20-50	37-79
S8	3.30	20-50	37-79
S7	3.42	20-50	37-79
S1 & Warrawoona	3.47	5-6	23-39

Table 1: Archean spherule layers. The layer thickness and age estimates for S5-S8 come from (Lowe et al., 2014) while all others are from Glass and Simonson (2012). The layers with multiple names are layers found at multiple localities that were likely created by the same impact (Glass and Simonson, 2012). For these "multiple" layers we report the entire range of layer thicknesses. The aggregate thickness is an estimate of how thick a layer composed of closely packed spherules would be. Aggregate thickness is the same as reduced layer thickness used in (Johnson and Melosh, 2012b). The impactor diameter is then calculated based on layer thickness using the same method as Johnson and Melosh (2012b).

By convolving the cumulative number of impacts from Figure 2 with the assumed probability of layer preservation and discovery, we can estimate the number of spherule

200 layers that a given bombardment history predicts. Note, the spherule layer record does
201 not rule out a scenario where the impactor flux was high 2.44-2.68 Ga, low from 2.68-3.2
202 Ga, and high from 3.2-3.5 Ga. However, such a bombardment history is inconsistent with
203 any of the dynamical models we consider (Bottke et al., 2012; Minton and Malhotra,
204 2010) and the terrestrial cratering record provides no evidence of periodic increases in
205 impactor flux (Bailer-Jones, 2011). On shorter time scales, however, asteroid disruption
206 events can produce increases in the flux of terrestrial impactors, as demonstrated by the
207 formation of the Flora asteroid family, which has been linked to an increased impactor
208 flux in the Ordovician (Nesvorný et al., 2007). It is unclear whether even larger
209 disruption events could deliver enough material to explain the formation of the Archean
210 spherule layers.
211
212 In Figure 3, we compare the flux implied by the four layers that formed 2.44-2.68 Ga to
213 the various bombardment histories shown in Figure 2. Assuming the spherule layers are
214 made by the smallest impactor sizes given in Table 1 and including the entire range of
215 random variation implied by Poisson statistics (vertical error bars $\sqrt{N}$), the spherule
216 layers are consistent with all the bombardment histories in Figure 2 including a constant
217 flux scenario. At the large end of the size range in Table 1, the spherule layers imply a
218 flux from 2.44-2.68 Ga that is more than 10 times higher than the current impactor flux.
219 At the low end of the size estimates from Table 1, however, the flux from 2.44-2.68 Ga is
220 consistent with even the current day flux.
221

222 In Figure 4, we compare the flux implied by the eight layers that formed 3.2-3.5 Ga to the
223 various bombardment histories shown in Figure 2. We find the spherule layers are
224 consistent with a flux significantly higher than any bombardment history in Figure 4.
225 Assuming the destabilization of the E-belt occurred at 4.1 Ga the E-belt flux during the
226 time of spherule layer formation is 2.1 times the current impactor flux. Note that E-belt
227 flux refers to the flux of impactors from the extension of the asteroid belt alone as shown
228 in Figure 2. Assuming the E-belt model is correct, the E-belt flux is in addition to some
229 background flux of material coming from the main belt. In Figures 3 and 4 we plot the
230 sum of the E-belt flux and the constant flux model. In the text however, we also consider
231 adding the E-belt flux to the decreasing flux of Minton and Malhotra (2010). If we
232 instead assume the E-belt destabilized 3.9 Ga, the E-belt flux is 5.1 times higher than the
233 current impactor flux during the period of spherule layer formation. The average flux
234 from the decreasing flux model is 5.8 times the constant flux model. We find that a total
235 impactor flux that is ~20-40 times the current, constant, impactor flux is required to
236 explain the Archean Spherule layers (dashed lines; Figure 4). We note the SFD inferred
237 from the spherule layers looks different from that of the main belt; we will return to this
238 in section 4.
239
240 Assuming the flux from the main belt is given by the constant flux model, the E-belt flux
241 would need to be 19-39 times the current impactor flux from 3.2-3.5 Ga to produce the
242 spherule layers that formed during this period. This corresponds to 9.0-19 times the E-
243 belt flux assuming destabilization occurred 4.1 Ga and 3.7-7.6 times if destabilization
244 occurred 3.9 Ga. If instead we assume the flux from the main belt is given by the

decreasing flux of Minton and Malhotra (2010), the E-belt flux would need to be 14-34 times the current current impactor flux from 3.2-3.5 Ga to produce the spherule layers that formed during this period. This corresponds to 6.7-16 times the E-belt flux assuming destabilization occurred 4.1 Ga and 2.7-6.7 times if destabilization occurred 3.9 Ga. The Hungaria asteroids are thought to be the only survivors of the E-belt (Bottke et al., 2012). Because the current population of Hungarias is so small, statistics allow an E-belt flux that was a factor of two higher than the nominal case (Bottke et al., 2012). Even with a doubling in flux, the E-belt flux is too low to explain the formation of the Archean spherule layers.

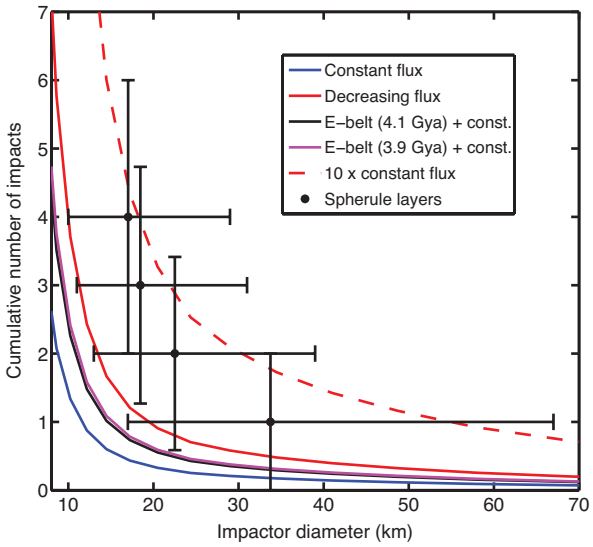

Figure 3: Cumulative number of impacts larger than a given size plotted as a function of impactor diameter. The curves all represent the number of impacts between 2.44-2.68 Ga predicted by different dynamical models as indicated by the legend. The black and purple curves are the cumulative number of impacts from the E-belt added to the number expected from the constant flux scenario. The points with error bars represent the range of SFDs allowed by the spherule layer data from Table 1. The horizontal error bars connect the two SFDs assuming the minimum and maximum size estimates in Table 1. The vertical error bars assume Poisson statistics (1-σ error of $\sqrt{N}$ where N is the number of layers). Although these errors should technically be on the flux estimates they provide a sense of the ranges of impactor flux that could explain the abundance of spherule layers.

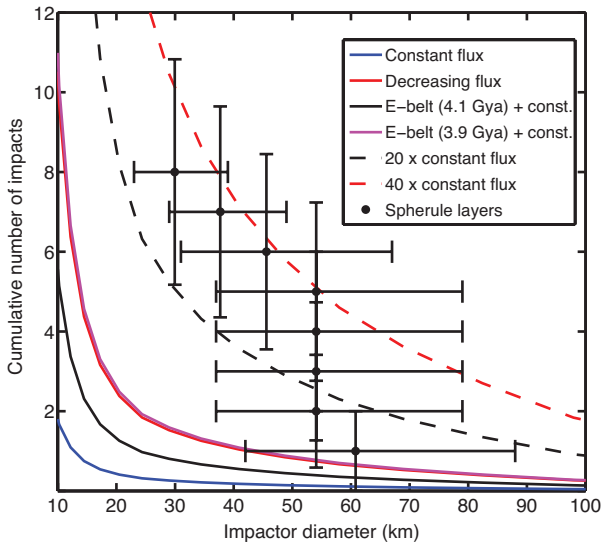

Figure 4: Cumulative number of impacts larger than a given size plotted as a function of impactor diameter. The curves all represent the number of impacts between 3.2-3.5 Ga predicted by different dynamical models as indicated by the legend. The black and purple curves are the cumulative number of impacts from the E-belt added to the number expected from the constant flux scenario. The points with error bars represent the range of SFDs allowed by the spherule layer data from Table 1. The horizontal error bars connect the two SFDs assuming the minimum and maximum size estimates in Table 1. The vertical error bars assume Poisson statistics (1-σ error of $\sqrt{N}$ where N is the number of layers). Although these errors should technically be on the flux estimates they provide a sense of the ranges of impactor flux that could explain the abundance of spherule layers.

3 Crater scaling laws

A principal constraint used to test any impact flux model is the observed number of impact basins on Earth and the Moon. For example, Bottke et al. (2012) used the observed number of post-LHB "Chicxulub-scale" (D > 160 km) impact craters on Earth and the Moon as a test of their E-belt impact flux model. Crucially, to convert a theoretical impactor SFD into a crater SFD requires a recipe for predicting the size of the final crater formed by the collision of an impactor of known mass, velocity and angle

289 onto a planetary surface of known density and gravity. While this procedure is
290 straightforward for small, simple bowl-shaped craters, it is complicated greatly by the
291 process of crater modification (collapse) that becomes increasingly prevalent as crater
292 size increases and internal crater morphology departs more and more from a simple bowl.
293 As a result, several frameworks have been described and used in the literature, based on
294 different observational constraints and assumptions about the nature of crater collapse, to
295 predict the amount of enlargement that occurs during crater modification. While
296 misapplication of these different approaches provides scope for disparate results, here we
297 show that their careful application provides a reasonably consistent relationship (<10%
298 discrepancy) between crater size and impactor properties that is in excellent agreement
299 with recent numerical models of terrestrial crater formation. In section 5, we apply this
300 framework to compare the flux inferred from spherule layers to the lunar cratering record.
301
302 Estimating crater size from impactor and target properties is conventionally done in two
303 steps. First, equations derived using the point-source approximation and dimensional
304 analysis relate impactor and target properties to the diameter of the so-called transient
305 crater (Holsapple, 1993; Holsapple and Schmidt, 1982). These equations are constrained
306 by laboratory-scale impact experiments (Schmidt and Housen, 1987) and numerical
307 models. As its name indicates, the transient crater is the short-lived bowl-shaped cavity
308 excavated during the early stages of impact, which is modified by gravity-driven collapse
309 of the transient crater walls and floor.
310

311 The diameter of the transient crater, D_{trans}, measured at the pre-impact target surface, is
312 given by the following equation from Collins et al. (2005) and references therein:

313 $$D_{trans} = 1.161 \left(\frac{\rho_{imp}}{\rho_{targ}}\right)^{\frac{1}{3}} D_{imp}^{0.78}\, v_{imp}^{0.44}\, g^{-0.22} \sin^{1/3}(\theta), \qquad (1)$$

314 where ρ_{imp} is impactor density, ρ_{targ} is target density, D_{imp} is impactor diameter, v_{imp}
315 is impact velocity, g acceleration due to gravity, and θ is the impact angle measure with
316 respect to the target surface (90° for a vertical impact and 0° for a grazing impact). All of
317 the quantities in Equation 1 are in MKS units. This equation is valid for gravity-scaled
318 craters, meaning the weight of the excavated material is the principal force arresting
319 crater growth. On Earth, Equation 1 is valid for impactors larger than about one meter in
320 diameter (Holsapple, 1993). This equation also assumes the impact is into a target with
321 no appreciable porosity. We note again that the impactor size, velocity and gravity
322 dependencies (exponents) in this equation are constrained by laboratory-scale impact
323 experiments (e.g., Schmidt and Housen, 1987).
324
325 The transient crater diameter is not equal to the final crater diameter. The bowl-shaped
326 transient crater is unstable and collapses under the influence of gravity. Scaling from
327 transient crater to final crater size is not experimentally constrained. On Earth, craters
328 larger than $D_{sc} \approx 2 - 4$ km have more complex morphologies, including central uplifts
329 and peak rings. These morphologies are attributed to uplift of the crater floor during wall
330 collapse (e.g., Melosh, 1989). Several scaling laws based on detailed observation of
331 craters and their ejecta, as well as reconstructions of transient crater geometry, have been
332 used to produce relationships between transient crater and final crater diameter (Croft,
333 1985; Holsapple, 1993; Schenk and McKinnon, 1985). Correct application of these

334 expressions requires careful attention to the definitions of pre- and post-collapse crater
335 diameters, measured either at the level of the pre-impact surface or at the crater rim. As
336 Equation (1) defines the diameter at the pre-impact level, here we take care to relate that
337 measure of the transient crater (D_{trans}) to the final crater diameter measured at the rim
338 crest (D_{final}). The increase in crater diameter therefore results from both crater
339 enlargement by rim collapse and the inward-dipping slope of the rim.
340
341 Grieve and Garvin (1984) describe a well-tested geometric model for the collapse of
342 simple craters. This model, under the assumption of a 5-10% increase in the volume of
343 the collapsing rim material to account for shear bulking, suggests that the ratio $\gamma = \frac{D_{final}}{D_{trans}}$
344 (the final crater diameter measured at the rim crest divided by the transient crater
345 diameter measured at the pre-impact level) is 1.23-1.28. This brackets the $\gamma = 1.25$
346 assumed by Collins et al. (2005).
347
348 Several authors (e.g., Croft, 1985; Schenk and McKinnon, 1985, Holsapple, 1993)
349 describe similar geometric models for complex crater formation. To combine with
350 Equation (1), these equations should take the general form:
351 $$D_{final} = A{D_{sc}}^{-\eta}{D_{trans}}^{1+\eta} \quad (2)$$
352 where D_{sc} is the final rim diameter at the simple-to-complex transition and A and η are
353 constants. However, to compare these models it is crucial that a consistent definition of
354 D_{trans} is used. Although these equations all seek to relate final crater diameter to
355 transient crater diameter they are most informatively compared when expressed in the
356 form:

$$\frac{D_{final}}{D_{eqs}} = \left(\frac{D_{eqs}}{D_{sc}}\right)^{\eta} \quad (3)$$

where D_{sc} is the final rim diameter at the simple-to-complex transition, $D_{eqs} = \gamma D_{trans}$ is the final rim diameter of the "equivalent simple crater" and η is the same constant as in Equation (2). This form is convenient because the enlargement factor is 1 at the simple-to-complex transition and increases monotonically as crater size increases (the equation does not apply for $D_{eqs} < D_{sc}$). When expressed in this form, the three geometric models of complex crater collapse in wide use can be described by η and $\gamma = A^{\frac{1}{1+\eta}}$, the ratio of final to transient crater diameter for simple craters (Table 2).

Table 2 Complex crater enlargement model parameters

Model	η	A	γ
Croft (1985)	**0.123-0.234**	**1**	1
Croft (1985); modified	**0.123-0.234**	1.28-1.32	**1.25**
Schenk and McKinnon (1985)[1]	**0.13**	**1.17**	1.15
" modified	**0.13**	1.29	**1.25**
Holsapple (1993)	**0.086**	1.35	**1.32**

Bold values are specified; remaining parameter is implied.
[1]Description of the Schenk and McKinnon (1985) model is also presented in McKinnon and Schenk (1985) and McKinnon et al. (2003).

A comparison of the complex crater collapse models of Croft (1985), Schenk and McKinnon (1985) and Holsapple (1993) reveals that they (apparently) make quite disparate assumptions regarding crater enlargement for craters with diameters below the simple-complex transition, ranging from $\gamma = 1$ (i.e., no collapse; Croft, 1985) to $\gamma =$

375 1.32 (Holsapple, 1993). The assumption of $\gamma = 1$ is not appropriate for two reasons.
376 First, both geometric and numerical models of simple crater formation show that
377 substantial enlargement occurs in large simple craters via debris sliding of the over-
378 steepened transient crater rim walls. Second, a value of $\gamma = 1$ only makes sense if the
379 transient crater diameter is measured at the rim; according to the transient crater diameter
380 definition preferred here, γ must be 5-10% larger to account for the slope of the transient
381 crater rim above the preimpact surface. This latter observation also applies to the value of
382 $\gamma = 1.15$ adopted by Schenk and McKinnon (1985), because they also defined the
383 transient crater diameter at the transient crater rim. In this case, the implied value of γ, as
384 defined here, would be about ≈ 1.24 (Figure 7 in Schenk and McKinnon, 1985). To
385 adjust both of these models to use transient crater diameter at the pre-impact level (and
386 account for simple crater collapse) we have redefined the value of A in Equation (2) for
387 each model assuming $\gamma = 1.25$, as suggested by the geometric model of simple crater
388 collapse proposed by Grieve and Garvin (1984) (modified model parameters in Table 2).
389 We note that as this modification leaves Equation (3) unchanged, it has no consequence
390 for how each model was derived from observations. Holsapple (1993) based his
391 assumption of $\gamma = 1.32$ (which adopts the same transient crater diameter definition as
392 used here) on measured shapes and rim profiles of craters produced in small-scale
393 laboratory cratering experiments, which are often regarded as "frozen" transient craters.
394 Although this is somewhat larger than 1.25 it has a sound basis and serves as a useful
395 measure of uncertainty in simple crater enlargement. We therefore retain it for our
396 analysis rather than modifying it to assume a consistent value of γ across all (modified)
397 models.

Figure 5 compares the five complex crater collapse models given by Equation 2 and parameters in Table 2. Both transient and final crater diameters are normalized to the simple-complex transition diameter D_{sc}. There is good agreement between the three modified models (solid lines) if the lower bound for complex crater enlargement of Croft (1985) is used. Adopting the upper bound of Croft (1985) would overestimate the final crater diameter by as much as 60% if that model was applied to the largest lunar basins. Also evident is the potential for a systematic discrepancy between models of ~30% in final crater diameter if inconsistent definitions of the transient crater diameter are used.

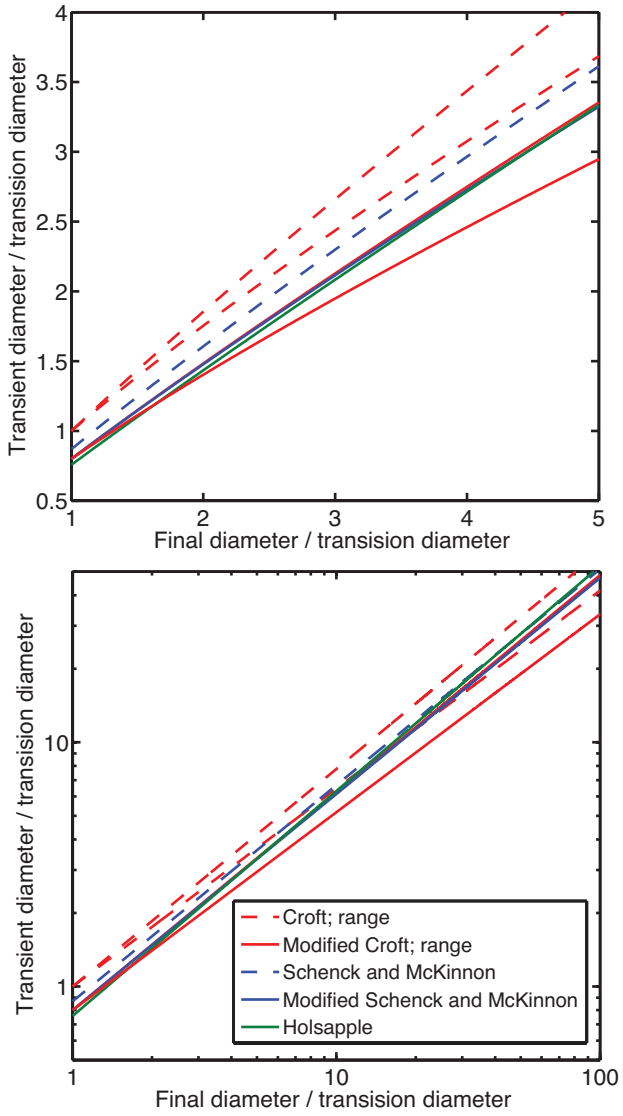

Figure 5 Comparison of complex crater enlargement scaling laws. Transient crater diameter normalized by the simple-complex transition diameter as a function of final (rim) diameter normalized in the same way. Dashed lines show the original models of McKinnon and Schenk (1985) and Croft (1985) in which the transient crater diameter is measured at the rim. Solid lines show the modified models in which transient crater diameter is measured at the pre-impact level, for use with transient crater scaling laws.

Another way to estimate final crater diameters is using detailed numerical models called hydrocodes or shock physics codes to directly model crater excavation and collapse. The iSALE shock physics code has been rigorously tested against experiment including impact and shock experiments in porous materials (Collins et al., 2011; Wünnemann et

al., 2006); oblique impact experiments into strong ductile materials (Davison et al., 2011); and thin plate jetting experiments (Johnson et al., 2014). The iSALE shock physics code includes detailed constitutive relations used to model the deformation of geologic materials (Collins et al., 2004). Recently Collins (2014) added a dilatancy model, which describes how deformation increases the porosity of geological materials. Using iSALE Collins (2014) modeled the formation of terrestrial craters from roughly 2-200 km in diameter by varying impactor diameter from 0.1-20 km in diameter. In addition to matching the observed morphology of craters including the transition from simple to complex craters and the transition from central-peak to peak-ring craters, these models also reproduced the observed gravity signature of terrestrial craters (Collins, 2014).

Figure 6 shows a comparison between the crater diameter predicted by scaling laws, (Equations 1 and 2), and the model crater diameters from Collins (2014). The scaling law for transient crater size (Equation 1) is derived from impact experiments and the scaling laws for final crater diameter (Equation 2) are derived from observation of craters and their ejecta, as well as reconstructions of transient crater geometry. Thus numerical models of crater formation and collapse act as an independent test of these scaling laws. We determine the rim location from the models by measuring the point of highest topography, measured with respect to the pre-impact surface. As rim topography tends to be smooth in the numerical simulations, introducing a small uncertainty in the exact rim location, the error bars in Figure 6 represent the innermost and outermost location where

441 the crater reaches 90% of this highest topography. Clearly, the simple scaling laws and
442 detailed models of crater formation are in excellent agreement.
443
444 Given the close correspondence between the numerical impact models and the (modified)
445 complex crater collapse scaling laws, and the consistency between scaling laws,
446 particularly those of Croft (1985; lower bound) and Schenk and McKinnon (1985), we
447 propose that the latter model be used to derive an equation for general use that relates
448 impactor and target properties directly to the final crater rim diameter by combining Eqs
449 1 and 2:

450 $$D_{fin} = 1.52 \left(\frac{\rho_{imp}}{\rho_{targ}}\right)^{0.38} D_{imp}^{0.88} v_{imp}^{0.5} g^{-0.25} D_{SC}^{-0.13} \sin^{0.38}(\theta) \quad (4)$$

451 All of the quantities in Equation 4 are in MKS units. Note that the value for the simple to
452 complex transition D_{SC} is target body specific and that Equation 4 is only valid for final
453 craters larger than D_{SC}. We note that the ~10% difference between various scaling laws
454 and numerical models (figure 6) can be used as a rough estimate of the error associated
455 with equation 4.
456
457 Figure 6 shows that craters formed in non-porous targets are larger than those that form
458 in porous targets. Producing a good match between observed sizes of lunar craters and
459 the current day population of impactors, based on observations of NEOs and the mian
460 asteroid belt, requires a transition from porous scaling to non-porous scaling at a crater
461 size around 0.5-10 km in diameter (Ivanov and Hartmann, 2007). Although, this does not
462 affect our estimates of the impactor sizes needed to create large craters, for completeness
463 we create an equation for final crater diameter that is appropriate for impacts into porous

targets. This equation uses the modified Schenk and McKinnon (1985) for transient to final crater scaling.

$$D_{fin} = 1.66 \left(\frac{\rho_{imp}}{\rho_{targ}}\right)^{0.38} D_{imp}^{0.94} v_{imp}^{0.38} g^{-0.19} D_{SC}^{-0.13} \sin^{0.38}(\theta) \quad (5)$$

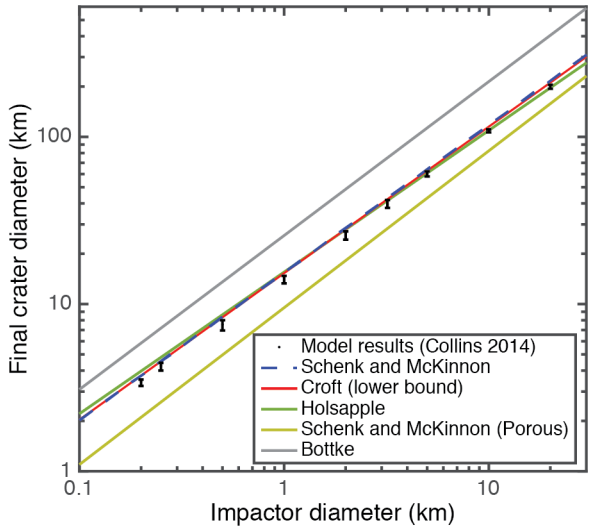

Figure 6: Comparison of numerical impact models and crater scaling laws. The solid curves were calculated using Equations 1 and 2, with parameters in Table 1, using the same impact conditions as those of the numerical impact models of Collins (2014), $v_{imp} = 15$ km/s, $\rho_{imp} = \rho_{targ}$, $\theta = 90°$, $g = 9.81$ m/s^2, and $D_{sc} = 4$ km. The points with error bars are the final crater diameters, for craters larger than D_{sc}, from Collins (2014). The main text describes how rim location and error bars are determined. The red curve shows the results obtained using the equations from the LPL calculator (equations described in text) and assuming, as Bottke et al. (2012, 2015) do, that an impactor of a given size produces a crater of the same size on both the Earth and the Moon. That is, $v_{imp} = 15$ km/s, $\rho_{imp} = \rho_{targ}$, $\theta = 90°$, $g = 1.67$ m/s^2, $D_{sc} = 18$ km.

For a typical E-belt impact with $v_{imp} = 22$ km/s, $\rho_{imp} \approx \rho_{target}$, $D_{sc} = 4$ km, and the most probable impact angle $\theta = 45°$, a 13.2-km diameter impactor is required to make a Chicxulub-sized crater, $D_{final} = 160$ km, on Earth. This impactor diameter is more than a factor of two larger than that assumed to produce Chicxulub-sized craters in tests of the

E-belt model (Bottke et al., 2012; 2015). E-belt impactors were initially assumed to have a SFD similar to the current main belt (Bottke et al., 2012; Minton et al., 2015b). Using the SFD of the main belt (Figure 1), we compare the number of 6 km diameter bodies to the number of 13.2-km diameter bodies. We find that the E-belt forms 71 craters larger than 160 km in diameter on Earth over 4.1 Gyr where Bottke et al. (2012) report that 523 should form. Thus, the E-belt model overstates its consequences by a factor of more than 7.4. If instead we assume E-belt impactors had a SFD similar to Near Earth Objects (NEOs), the same comparison indicates this factor is 9.7.

For the same impact conditions above, we find a 27-km diameter impactor is required to form a 300-km diameter impact basin on Earth. Using the SFD of the main belt, we compare the number of 6-km diameter bodies to the number of 27-km diameter bodies. We find that the E-belt creates 22 basins larger than 300 km in diameter on Earth over 4.1 Gyr where Bottke et al. (2012) reports that 154 such basins should form.

Using Equation 4 with lunar gravity $g = 1.62$ m/s^2, $D_{SC} = 15$ km appropriate for the Moon (Croft, 1985), $v_{imp} = 22$ km/s, $\rho_{imp} \approx \rho_{target}$, and the most probable impact angle $\theta = 45°$, we find 9.7-km and 19.7-km diameter impactors are required to create 160-km and 300-km craters on the Moon, respectively. Using the main-belt SFD we compare the number of 6-km diameter bodies to the number of 9.7-km and 19.7-km diameter bodies. We find that the nominal E-belt model only creates 2 lunar craters larger than 300 km and 8.7 craters larger than 160 km in diameter in 4.1 Gyr compared to the 9.1 and 31 reported by Bottke et al. (2012), respectively.

Bottke et al. (2012; 2015) use the following LPL online calculator to estimate final crater diameter produced by a given impact (http://www.lpl.arizona.edu/tekton/crater.html). The source code reveals that the calculator uses Equation 1 to calculate the transient crater diameter but the final crater diameter is calculated using $D_{final} = D_{eqs}^{1.18}/D_{SC}^{0.18}$ (Croft, 1985), where the equivalent simple crater diameter is assumed to be $D_{eqs} = 1.56\, D_{trans}$ (i.e., $\gamma = 1.56$). Hence, this approach overestimates both the enlargement factor owing to simple crater collapse (γ) and the additional enlargement owing to complex crater collapse (through the exponent η). Another minor effect that contributes to the overestimate of crater sizes in Bottke et al. (2012; 2015) is the assumption that an impactor of a given size makes a crater of the same size on both the Earth and the Moon. More precisely, Bottke et al. (2012; 2015) use $g = 1.67$ m/s^2 and $D_{SC} = 18$ km for both the Earth and Moon.

Johnson and Bowling (2014) estimated the expected terrestrial cratering record based on different terrestrial bombardment histories. They reported that the impactors from the E-belt alone could create six craters larger than 85 km in diameter that may have survived until today (Johnson and Bowling, 2014). Unfortunately, Johnson and Bowling (2014) assumed that the number of Chicxulub-sized craters the E-belt can form reported by Bottke et al. (2012) was correct. Thus, they overestimate the contribution of the E-belt to the terrestrial cratering record by a factor of 7.5-10. Considering this, we conclude that the nominal E-belt would at most create a single crater larger than 85 km in diameter that survives to the current day on Earth. At least 6 craters of this size have been recognized

531 on Earth. Because Bottke et al. (2012) did not report the impactor diameter assumed to
532 make Chicxulub-sized craters, any paper using their flux estimates likely overestimates
533 the E-belt flux by a factor of ~7.5-10.
534
535 **4 The size distribution of ancient terrestrial impactors**
536 We have assumed that the SFD of impactors that created the spherule layers was
537 equivalent to the main belt SFD. However, recent work shows that bombarding the Moon
538 with a main-belt-like SFD would create an overabundance of mega-basins, craters with
539 diameters greater than 1200 km (Minton et al., 2015b). An impactor SFD that agrees with
540 the lunar cratering record has ~630 impactors larger 5.5 km in diameter for every one
541 impactor larger than 70 km in diameter (Minton et al., 2015b). Two scenarios that adhere
542 to this constraint are shown by the grey diamonds (scenario 1) and blue squares (scenario
543 2) in Figure 7. We propose two potential SFDs that are consistent with both the lunar
544 cratering record and the spherule layer record. These SFDs also minimize differences
545 between the proposed SFDs and the main-belt SFD.
546
547 The grey "Proposed SFD 1" curve in Figure 7 shows a SFD that is main-belt-like up to
548 ~50 km in diameter with an abrupt steepening above 50 km. This SFD is similar to the
549 SFDs produced by catastrophic disruption of large parent bodies (Durda et al., 2007). In a
550 catastrophic disruption SFD the steepening occurs at diameters near the largest remaining
551 fragment size (Durda et al., 2007). This does not match the predictions of the E-belt
552 model (Bottke et al., 2015; 2012), but is potentially consistent with a giant impact ejecta
553 origin for the LHB impactors and the impactors that created the Archean spherule layers

554 (Minton et al., 2015a; Volk and Gladman, 2015). Although Figure 3 only includes
555 spherule layers corresponding to impactors that are ~20-30 km in diameter, figure 4
556 includes spherule layers that correspond to impactors that are ~30-60 km in diameter (ie.
557 the same size range where proposed SFD 1 becomes steep). The impactor SFD from
558 spherule layers shown in figure 4 does show some steepening at the larger impactor sizes.
559 This disagreement between the main-belt SFD and spherule layer SFD shown in figure 4
560 may be further indication that the population of ancient terrestrial impactors was
561 something like Proposed SFD 1.
562
563 The blue "Proposed SFD 2" is main-belt like for impactors larger than 20 km in diameter
564 and steeper than the main belt for impactors smaller than 30 km in diameter. If the E-
565 belt had a significantly different collisional history than the main belt, this relative SFD
566 could be consistent with the population of E-belt impactors (Bottke et al., 2015).
567 However, the absolute E-belt flux would still be too low to explain the formation of the
568 Archean spherule layers. "Proposed SFD 2" is similar to the SFD of asteroid families
569 created by cratering on a large parent body (Durda et al., 2007). Because little is known
570 about the initial SFD of giant impact ejecta, this SFD is also potentially consistent with
571 giant impact ejecta (Jackson et al., 2014). Clearly, detailed modeling of the formation and
572 collisional evolution of giant impact ejecta is required to determine if a giant impact
573 ejecta origin for the LHB is consistent with constraints on the ancient impactor
574 population.

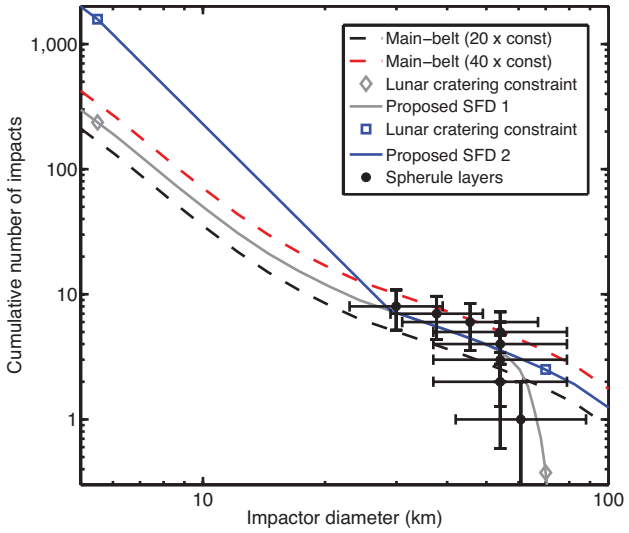

575

576 **Figure 7:** Log-log plot of the cumulative number of impacts larger than a given size
577 plotted as a function of impactor diameter. The dashed red and black curves are the same
578 as those described in Figure 4 and represent the main-belt SFD. The black points with
579 error bars represent the SFD from spherule layers that formed between 3.2-3.5 Ga as
580 described in Figure 4. The grey diamonds show the relative number of impactors larger
581 than 70 km in diameter and 5.5 km in diameter needed to explain the lunar cratering
582 record. The blue squares show the same constraint but with a higher total flux.
583

584

585 The spherule record along with lunar cratering constraints based on the apparent lack of
586 mega-basins (Minton et al., 2015b) allow for a range of possible impactor SFDs (Figure
587 7). These SFDs, however, make completely different predictions for the number of
588 smaller craters we expect to find on the Moon. Fasset and Minton (2013) recently
589 compiled a variety of constraints based on the lunar cratering record (Neukum et al.,
590 2001; Stöffler and Ryder, 2001), putting them all in terms of the rate at which craters
591 larger than 20 km in diameter form on the Moon (Figure 8).

592

593 To compare the spherule layer record to the lunar cratering record, we first estimate the
594 impactor size required to a make a 20-km diameter crater. Using Equation 4 with lunar
595 gravity $g = 1.62$ m/s^2 and $D_{SC} = 15$ km appropriate for the Moon (Croft, 1985), $v_{imp} =$
596 16 km/s typical for the Moon (Yue et al., 2013), $\rho_{imp} \approx \rho_{target}$, and the most probable
597 impact angle $\theta = 45°$, we find a 1.1 km diameter impactor is required to make a 20 km
598 diameter crater on the Moon. As shown in section 2, the spherule layers that formed
599 between 2.44-2.8 Ga and 3.2-3.5 Ga are consistent with and impactor flux that is 1-10
600 times and 20-40 times the current day flux, respectively, for very large impactors (~10-
601 100 km in diameter). To estimate the flux of impactors larger than 1.1 km in diameter, we
602 then extrapolate to smaller impactor sizes using proposed SFD 1 (black boxes) and
603 proposed SFD 2 (blue boxes) (where proposed SFD 2 is assumed to be main-belt like for
604 impactors smaller than 5.5 km in diameter).
605
606
607

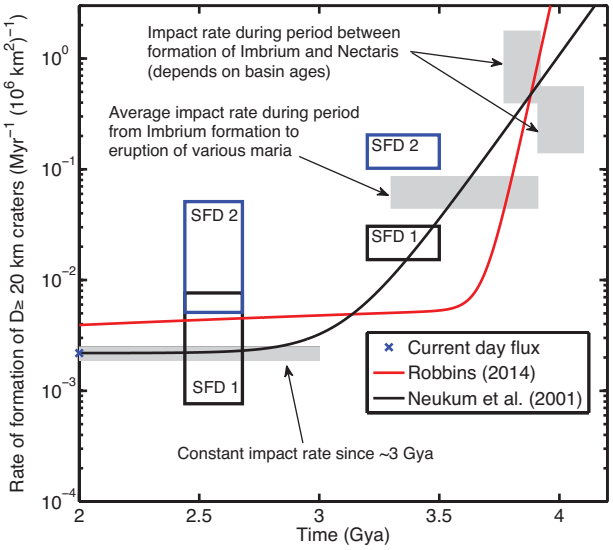

608

609 **Figure 8:** Estimates of impactor flux on the Moon. The filled grey boxes are estimates
610 made by Fassett and Minton (2013). The blue star plotted at 2 Ga is the current impactor
611 flux according to observations of NEOs. The comparison of flux based on spherule layers
612 to lunar cratering record assumes that 17 impactors of a given size hit the Earth for every
613 one that hits the Moon (Bottke et al. 2012). The flux implied by the spherule layers is
614 estimated assuming proposed SFD 1 (black boxes) and proposed SFD 2 (blue boxes). The
615 red and black curves are best fit estimates from Neukum et al. (2001) and Robbins
616 (2014), respectively. The curves were scaled from the rate of formation of 1 km diameter
617 craters by normalizing to the current rate at which 20-km diameter craters form on the
618 Moon.
619

620 When using proposed SFD 1, the rate of formation of 20 km diameter craters is consistent
621 with the lunar crater chronology of Neukum et al. (2001) (Figure 8). Whereas, if we use
622 proposed SFD 2 the implied flux is roughly an order of magnitude higher than the
623 Neukum lunar cratering chronology (Figure 8). On this basis we argue that proposed
624 SFD 1 is more consistent with the lunar chronology than proposed SFD 2. Although
625 proposed SFD 1 does better than proposed SFD 2, neither SFD fits the chronology of
626 Robbins (Robbins, 2014). This may imply that the Neukum (2001) chronology is more
627 representative of the terrestrial impactor flux.

628

5 Discussion:

We note that the chronology of Robbins (2014) is in disagreement with the average rate of formation of 20-km diameter craters on the lunar maria (Figure 8, Fassett and Minton 2013). Although, Robbins (2014) was careful to remove clusters of secondary craters, distant secondary craters may be spatially homogeneous (McEwen and Bierhaus, 2006). The only way to ensure secondary craters are omitted is to count only craters larger than ~1 km in diameter (McEwen and Bierhaus, 2006), but Robbins (2014) focuses on craters 1 km in diameter and smaller. Consequently, we prefer the grey boxes in Figure 8 as constraints, as these flux estimates are based on the number of 20-km diameter craters (Fasset and Minton 2013). Clearly there are some significant uncertainties associated with interpretations of the lunar crater record.

The exceptional agreement between the current rate of formation of lunar craters larger than 20 km in diameter implied by observations of NEO's and estimates based on lunar craters provides an independent validation of the crater scaling laws discussed in section 3 (Figure 8). Recent careful work interpreting the terrestrial cratering record by Hughes (2000) suggest craters larger than 20 km in diameter were created at a rate of (3.46 ± 0.30) x 10^{-15} km^{-2} yr^{-1} over the past 125±20 Myr. This is in excellent agreement with crater scaling laws and estimates of the current day impactor flux based on observations of NEO's. Within the reported error, the commonly used (5.6 ± 2.8) x 10^{-15} km^{-2} yr^{-1} (Grieve, 1998) for the formation rate of craters larger than 20 km in diameter is consistent with estimate of Hughes (2000).

652 Another potential source of error come from uncertainties in the estimates of the sizes of
653 impactors that created the Archean spherule layers. Estimates based on layer thickness
654 and extraterrestrial material content generally agree that the centimeters to 10's of
655 centimeters thick Archean spherule layers were created by impactors that were ~10-90
656 km in diameter (Johnson and Melosh, 2012b; Kyte et al., 2003; Lowe et al., 2003, 2014;
657 Lowe and Byerly, 2015). However, estimates based on extraterrestrial material content
658 may be affected by the heterogeneous distribution of Ni-rich chromium spinel which
659 accounts for the bulk of the enrichment in platinum group elements. Additionally, many
660 layers show signs of dilution, redeposition by surface processes, and tectonic deformation
661 potentially affecting the thickness estimates reported in table 1 (Lowe et al., 2003). It is
662 also possible that some of the layers are not global vapor plume layers but are more
663 proximal ejecta like deposits from the Sudbury or Vredefort impacts (Cannon et al.,
664 20010; Huber et al., 2014a,b). This has already been suggested for the Carawine,
665 Jeerinah, and Dales Gorge spherule layers based on the characteristics of their spherules
666 and related melt particles (Simonson et al., 2000; Jones-Zimberlin et al., 2006; Sweeney
667 and Simonson, 2008). One test of the estimates of impactor size comes from the
668 comparison to the lunar cratering record. For example, if the impactor flux implied by the
669 Archean spherule layers was well above that implied by the lunar cratering record this
670 may imply impactor sizes are consistently over estimated. Figure 8 shows that for a
671 reasonable impactor size frequency distribution, it is possible to reconcile the impactor
672 flux implied by spherule layers with flux estimates based on the lunar cratering record.
673

When an impactor component is recognized in a spherule layer, its composition can act as a further constraint on LHB models. The Chromium isotopes in S2, S3, and S4 (from 3.2-3.5 Ga) all imply they were formed by carbonaceous chondrite impactors (Kyte et al., 2003). This is in contrast to the younger layers that formed between 2.44-2.68 Ga, which show a variety of compositions consistent with E-chondrites, Martian meteorites, or ordinary chondrites (Simonson et al., 2009). The compositions of the older layers, which imply an impactor flux ~20-40 the current impactor flux, may appear inconsistent with a giant impact origin for the LHB (Minton et al., 2015a; Volk and Gladman, 2015). However, if ejecta from a giant impact on Mars created the spherule layers, the common composition of S2, S3, and S4 could be explained by one of the bodies involved in the giant impact being a large carbonaceous chondrite, potentially a body similar to Ceres.

It is intriguing that the Martian moons, Phobos and Deimos, appear to be a combination of Martian and carbonaceous chondrite material (Citron et al., 2015). Moreover, Citron et al. (2015) suggest that Phobos and Deimos were the result of the putative Borealis-forming giant impact (Andrews-Hanna et al., 2008). The return of samples from Mars, Phobos, and Deimos along with detailed isotopic analysis could conceivably detect the signature of the putative giant impactor. Regardless of the source of the ancient impactors, the terrestrial spherule layers, when coupled with the lunar cratering record, clearly offer valuable clues about the population of ancient terrestrial impactors.

Acknowledgments:

We thank Christian Koeberl and an anonymous reviewer for their helpful reviews. We also thank H. Jay Melosh for fruitful discussion and comments on an earlier version of this manuscript.

Andrews-Hanna, J.C., Zuber, M.T., Banerdt, W.B., 2008. The Borealis basin and the origin of the martian crustal dichotomy. Nature 453, 1212–1215, doi:10.1038/nature07011

Bailer-Jones, C.A.L., 2011. Bayesian time series analysis of terrestrial impact cratering. Month. Not. R. Astr. Soc. 416, 1163–1180, doi:10.1111/j.1365-2966.2011.19112.x

Bottke, W.F., Marchi, S., Vokrouhlický, D., Robbins, S., Hynek, B., Morbidelli, A., 2015. New insights into the Martian late heavy bombardment. Lunar Planet. Sci. Conf. XLVI, #1484.

Bottke, W.F., Vokrouhlický, D., Minton, D., Nesvorný, D., Morbidelli, A., Brasser, R., Simonson, B., Levison, H.F., 2012. An Archaean heavy bombardment from a destabilized extension of the asteroid belt. Nature 485, 78–81, doi:10.1038/nature10967

Cannon, W.F., Schulz, K.J., Horton, J.W. Jr, Kring, D.A., 2010. The Sudbury impact layer in the Paleoproterozoic iron ranges of northern Michigan, USA. Geol. Soc. Am. Bull 122, 50–75, doi:10.1130/B26517.1

Citron, R.I., Genda, H., Ida, S., 2015. Formation of Phobos and Deimos via a giant impact. Icarus 252, 334–338, doi:10.1016/j.icarus.2015.02.011

Collins, G.S., 2014. Numerical simulations of impact crater formation with dilatancy. J. Geophys. Res. Planets 119, doi:10.1002/2014JE004708

Collins, G.S., Melosh, H.J., Ivanov, B.A., 2004. Modeling damage and deformation in impact simulations. Meteor. Planet. Sci. 39, 217–231.

Collins, G.S., Melosh, H.J., MARCUS, R.A., 2005. Earth Impact Effects Program: A Web- based computer program for calculating the regional environmental consequences of a meteoroid impact on Earth. Meteor. Planet. Sci. 40, 817–840, doi:10.1111/j.1945-5100.2005.tb00157.x

Collins, G.S., Melosh, H.J., Wünnemann, K., 2011. Improvements to the ε-α porous compaction model for simulating impacts into high-porosity solar system objects. International Journal of Impact Engineering 38, 434–439, doi:10.1016/j.ijimpeng.2010.10.013

Croft, S.K., 1985. The scaling of complex craters. J. Geophys. Res. 90, 828–C842, doi:10.1029/JB090iS02p0C828

Davison, T.M., Collins, G.S., Elbeshausen, D., Wünnemann, K., Kearsley, A., 2011. Numerical modeling of oblique hypervelocity impacts on strong ductile targets. Meteor. Planet. Sci. 46, 1510–1524, doi:10.1111/j.1945-5100.2011.01246.x

Durda, D.D., Bottke, W.F., Nesvorný, D., Enke, B.L., Merline, W.J., Asphaug, E.,

734 Richardson, D.C., 2007. Size–frequency distributions of fragments from SPH/N-
735 body simulations of asteroid impacts: Comparison with observed asteroid families.
736 Icarus 186, 498–516, doi:10.1016/j.icarus.2006.09.013

737 Fassett, C.I., Minton, D.A., 2013. Impact bombardment of the terrestrial planets and the
738 early history of the Solar System. Nature Geosci. 6, 520–524, doi:10.1038/ngeo1841

739 Glass, B.P., Simonson, B.M., 2012. Distal impact ejecta layers: Spherules and more.
740 Elements 8, 43–48, doi:10.2113/gselements.8.1.43

741 Gomes, R., Levison, H.F., Tsiganis, K., Morbidelli, A., 2005. Origin of the cataclysmic
742 Late Heavy Bombardment period of the terrestrial planets. Nature 435, 466–469,
743 doi:10.1038/nature03676

744 Grieve, R.A.F., 1998. Extraterrestrial impacts on Earth: The evidence and the
745 consequences. Geol. Soc., Lond., Sp. Pub. 140, 105–131,
746 doi:10.1144/GSL.SP.1998.140.01.10

747 Grieve, R. A. F., Garvin, J. B., 1984. A geometric model for excavation and modification
748 at terrestrial simple impact craters. J. Geophys. Res. 89, 11561–11572,
749 doi:10.1029/JB089iB13p11561

750 Harris, A. W. , D'Abramo, G., 2015.The population of near-Earth asteroids. Icarus 257,
751 302–312 , doi: 10.1016/j.icarus.2015.05.004

752 Holsapple, K., 1993. The scaling of impact processes in planetary sciences. Ann. Rev.
753 Earth Planet. Sci. 21, 333–373, doi:10.1146/annurev.earth.21.1.333

754 Holsapple, K.A., Schmidt, R.M., 1982. On the scaling of crater dimensions. II - Impact
755 processes. J. Geophys. Res. 87, 1849–1870, doi:10.1029/JB087iB03p01849

756 Huber M., McDonald I., Koeberl C., 2014. Petrography and geochemistry of ejecta from
757 the Sudbury impact event. Meteor. Planet. Sci. 49, 1749-1768,
758 doi:10.1111/maps.12352

759 Huber M.S., Crne A.E., McDonald I., Hecht L., Melezhik V.A., Koeberl C, 2014. Impact
760 spherules from Karelia, Russia: Possible ejecta from the 2.02 Ga Vredefort impact
761 event. Geology 42, 375-378, doi: 10.1130/G35231.1

762 Hughes, D.W., 2000. A new approach to the calculation of the cratering rate of the Earth
763 over the last 125 ± 20 Myr. Mon. Not. R. Astr. Soc. 317, 429–437,
764 doi:10.1046/j.1365-8711.2000.03568.x

765 Ivanov, B. A., Hartmann, W. K., 2007. In Treatise on Geophysics Vol. 10 Planets and
766 Moons (ed. Schubert, G.).Elsevier. 202–242, doi:10.1016/b978-044452748-6.00158-
767 9

768 Jackson, A.P., Wyatt, M.C., Bonsor, A., Veras, D., 2014. Debris froms giant impacts
769 between planetary embryos at large orbital radii. Mon. Not. R. Astr. Soc. 440, 3757–
770 3777, doi:10.1093/mnras/stu476

771 Johnson, B.C., Bowling, T.J., 2014. Where have all the craters gone? Earth's
772 bombardment history and the expected terrestrial cratering record. Geology 42, 587–
773 590, doi:10.1130/G35754.1

774 Johnson, B.C., Bowling, T.J., Melosh, H.J., 2014. Jetting during vertical impacts of
775 spherical projectiles. Icarus 238, 13–22, doi:10.1016/j.icarus.2014.05.003

776 Johnson, B.C., Melosh, H.J., 2012a. Formation of spherules in impact produced vapor
777 plumes. Icarus 217, 416–430, doi:10.1016/j.icarus.2011.11.020

778 Johnson, B.C., Melosh, H.J., 2012b. Impact spherules as a record of an ancient heavy
779 bombardment of Earth. Nature 485, 75–77, doi:10.1038/nature10982

780 Johnson, B.C., Melosh, H.J., 2014. Formation of melt droplets, melt fragments, and
781 accretionary impact lapilli during a hypervelocity impact. Icarus 228, 347–363,
782 doi:10.1016/j.icarus.2013.10.022

783 Jones-Zimberlin, S., Simonson B.M., Kreiss-Tomkins, D., Garson, D., 2006, Using
784 impact spherule layers to correlate sedimentary successions: a case study of the
785 Neoarchean Jeerinah layer (Western Australia). So. Afr. J. Geol. 109, 245-261,
786 doi:10.2113/gssajg.109.1-2.245

787 Koeberl, C., Schulz, T., Reimold, W.U., 2015a. Remnants of Early Archean Impact
788 Deposits on Earth: Search for a Meteoritic Component in the BARB5 and CT3 Drill
789 Cores (Barberton Greenstone Belt, South Africa). Procedia Engineering 103, 310-
790 317, doi:10.1016/j.proeng.2015.04.052

791 Koeberl, C., Schulz, T., Ozdemir, S., Mohr-Westheide, T., Reimold, W.U., Hofmann, A.,
792 2015b. Remnants of early Archean impact rvents on Earth: New studies on spherule
793 layers from the Barberton Mountain Land, South Africa. Early Solar System Impact
794 Bombardment III, #3017.

795 Kyte, F.T., Shukolyukov, A., Lugmair, G.W., Lowe, D.R., Byerly, G.R., 2003. Early
796 Archean spherule beds: Chromium isotopes confirm origin through multiple impacts
797 of projectiles of carbonaceous chondrite type. Geology 31, 283, doi:10.1130/0091-
798 7613(2003)031<0283:easbci>2.0.co;2

799 Le Feuvre, M., Wieczorek, M.A., 2011. Nonuniform cratering of the Moon and a revised
800 crater chronology of the inner Solar System. Icarus 214, 1–20,
801 doi:10.1016/j.icarus.2011.03.010

802 Lowe, D.R., Byerly, G.R., 2015. Geologic record of partial ocean evaporation triggered
803 by giant asteroid impacts, 3.29–3.23 billion years ago. Geology. doi:
804 10.1130/G36665.1

805 Lowe, D.R., Byerly, G.R., Kyte, F.T., Shukolyukov, A., Asaro, F., Krull, A., 2003.
806 Spherule beds 3.47-3.24 billion years old in Barberton Greenstone Belt, South
807 Africa: a record of large meteorite impacts and their influence on early crustal and
808 biological evolution. Astrobiology 3, 7-48.

809 Lowe, D.R., Byerly, G.R., Kyte, F.T., 2014. Recently discovered 3.42-3.23 Ga impact
810 layers, Barberton Belt, South Africa: 3.8 Ga detrital zircons, Archean impact history,
811 and tectonic implications. Geology 42, 747–750. doi:10.1130/G35743.1

812 McEwen, A.S., Bierhaus, E.B., 2006. The importance of secondary cratering to age
813 constraints on planetary surfaces. Ann. Rev. Earth Planet. Sci. 34, 535–567,
814 doi:10.1146/annurev.earth.34.031405.125018

McKinnon, W.B., Schenk, P.M., 1985. Ejecta blanket scaling on the Moon and-Inferences for projectile populations. Lunar Planet. Sci. Conf. XVI, 544–545.

McKinnon, W.B., Schenk, P.M., Moore, J.M., 2003. Goldilocks and the Three Complex Crater Scaling Laws. Workshop on Impact Cratering #8047.

Melosh, H.J., 1989. Impact cratering: A geologic process. Oxford University Press.

Minton, D.A., Jackson, A.P., Asphaug, E., Fassett, C.I., Richardson, J.E., 2015a. Debris From Borealis basin formation as the primary impactor population of Late Heavy Bombardment. #3033.

Minton, D.A., Malhotra, R., 2010. Dynamical erosion of the asteroid belt and implications for large impacts in the inner Solar System. Icarus 207, 744–757, doi:10.1016/j.icarus.2009.12.008

Minton, D.A., Richardson, J.E., Fassett, C.I., 2015b. Re-examining the main asteroid belt as the primary source of ancient lunar craters. Icarus 247, 172–190, doi:10.1016/j.icarus.2014.10.018

Mohr-Westheide, T., Reimold, W.U., Fritz, J., Koeberl, C., Salge, T., Hofmann, A., Schmitt, R.T., 2015. Discovery of extraterrestrial component carrier phases in Archean spherule layers: implications for estimation of Archean bolide sizes. Geology 43, 299-302.

Morbidelli, A., Marchi, S., Bottke, W.F., Kring, D.A., 2012. A sawtooth-like timeline for the first billion years of lunar bombardment. Earth Planet. Sci. Lett. 355-356, 144–151, doi:10.1016/j.epsl.2012.07.037

Nesvorný, D., Vokrouhlický, D., Bottke, W.F., Gladman, B., Häggström, T., 2007. Express delivery of fossil meteorites from the inner asteroid belt to Sweden. Icarus 188, 400–413, doi:10.1016/j.icarus.2006.11.021

Neukum, G., Ivanov, B.A., Hartmann, W.K., 2001. Cratering records in the inner solar system in relation to the lunar reference system. Space Sci. Rev. 96, 55–86, doi:10.1023/A:1011989004263

Robbins, S.J., 2014. New crater calibrations for the lunar crater-age chronology. Earth Planet. Sci. Lett. 403, 188–198, doi:10.1016/j.epsl.2014.06.038

Schenk, P.M., McKinnon, W.B., 1985. Dark halo craters and the thickness of grooved terrain on Ganymede. J. Geophys. Res. 90, 775.

Schmidt, R.M., Housen, K.R., 1987. Some recent advances in the scaling of impact and explosion cratering. Int.J. Impact Eng. 5, 543–560, doi:10.1016/0734-743x(87)90069-8

Simonson, B.M., Glass, B.P., 2004. Spherule Layers—Records of Ancient Impacts. Ann. Rev. Earth Planet. Sci. 32, 329–361, doi:10.1146/annurev.earth.32.101802.120458

Simonson B.M., Hornstein, M., Hassler S.W., 2000, Particles in late Archean Carawine Dolomite (Western Australia) resemble Muong Nong-type tektites. In: Impacts and the Early Earth (Gilmour, I., Koeberl, C., eds.), Springer-Verlag, 181-214.

Simonson, B.M., McDonald, I., Shukolyukov, A., Koeberl, C., Reimold, W.U., Lugmair,

G.W., 2009. Geochemistry of 2.63–2.49 Ga impact spherule layers and implications for stratigraphic correlations and impact processes. Precambrian Res. 175, 51–76, doi:10.1016/j.precamres.2009.08.004

Smit, J., 1999. The Global Stratigraphy of thr Cretaceous-Tertiary Boundary Impact Ejecta. Annu. Rev. Earth Planet. Sci. 27, 75–113, doi:10.1146/annurev.earth.27.1.75

Stöffler, D., Ryder, G., 2001. Stratigraphy and Isotope Ages of Lunar Geologic Units: Chronological Standard for the Inner Solar System. Space Sci. Rev. 96, 9–54, doi:10.1007/978-94-017-1035-0_2

Stuart, J.S., Binzel, R.P., 2004. Bias-corrected population, size distribution, and impact hazard for the near-Earth objects. Icarus 170, 295–311, doi:10.1016/j.icarus.2004.03.018

Sweeney, D., Simonson, B.M., 2008. Textural constraints on the formation of impact spherules: A case study from the Dales Gorge BIF, Paleoproterozoic Hamersley Group of Western Australia. Meteor. Planet. Sci. 43, 2073-2087, doi:10.1111/j.1945-5100.2008.tb00662.x

Volk, K., Gladman, B., 2015. Consolidating and Crushing Exoplanets: Did it happen here? arXiv:1502.06558. ApJ 806, L26, doi: 10.1088/2041-8205/806/2/L26

Wünnemann, K., Collins, G.S., Melosh, H.J., 2006. A strain-based porosity model for use in hydrocode simulations of impacts and implications for transient crater growth in porous targets. Icarus 180, 514–527, doi:10.1016/j.icarus.2005.10.013

Yue, Z., Johnson, B.C., Minton, D.A., Melosh, H.J., Di, K., 2013. Projectile remnants in central peaks of lunar impact craters. Nature Geosci. 6, 435–437, doi:10.1038/ngeo1828